Chapter 7 Role of Incommensurate Longitudinal Conical Modulation and Evidence for Another Spin-Glass Transition in $BaFe_{12}O_{19}$

7.1 Introduction

In the preceding two chapters, we showed that $BaFe_{12}O_{19}$ (BFO) exhibits four spin-glass transitions below 70 K even in the absence of any substitutional disorder. These spin-glass transitions were shown to be linked with the freezing of the transverse and longitudinal components of the spins. The two high-temperature spin-glass transitions in the powder samples were found to occur at slightly higher temperatures than those obtained by single-crystal measurements, as can be seen from the results given in chapters 5 and 6, respectively. Interestingly, these two spin-glass transitions are followed by two more spin-glass transitions at lower temperatures with $T_{SG} \lesssim 15$ K due to the freezing of the longitudinal and transverse components, respectively. As will be discussed in the next chapter 8, the appearance of these two transitions in the reverse order may be linked with the change in the exchange splitting of the e_g lines of the X-ray absorption spectra (XAS) at the O K-edge around 15 K, discussed in chapter 4. All these spin-glass transitions show large attempt relaxation time (τ_0) which lies in the cluster glass regime. However, our system is an ordered close-packed system unlike the conventional disordered or nanocrystalline systems where spin cluster can exist due to local segregation of the magnetic element. We have therefore not distinguished between cluster and spin-glass behaviour in our system. As mentioned in the previous chapters, short-range ordered spin clusters have been observed in geometrically frustrated systems due to local antiferromagnetic (AFM)correlations rather than due to segregation of magnetic ion/atom or reduction in size in the conventional systems [18,410,411].

To our knowledge, there are two real systems, Pr based metallic glasses [412] and site disordered $LuFe_2O_4$ [312,413], which show three spin-glass/cluster glass transitions. The first systems may have built-in quenched frozen-in disorder and a complex magnetic phase diagram. The second system $LuFeO_4$ has both Fe^{2+} and Fe^{3+} cations which are believed to be charge-ordered but this ordering may be inhomogeneous. Thus, both systems are disordered. Two spin/cluster glass transitions have been reported involving freezing of transverse and longitudinal components of the spin at two different temperatures (see e.g. Ref. [74]). Further, several disordered systems have been reported to exhibit spin-glass (see e.g. Ref. [380]) to cluster glass and cluster glass to spin-glass (see e.g. Ref. [414]) transitions also. Theoretical studies on disordered Heisenberg systems in the vicinity of the percolation threshold compositions predict occurrence of the successive freezing of transverse and longitudinal components of the spins leading to two spin-glass phases in coexistence with the long-range ordered (LRO) phase [65]. It has been shown that such a succession of two spin-glass transitions may occur in systems with low single-ion anisotropy [66,68], exchange anisotropy (not necessarily low) [236] and Dzyaloshinsky-Moriya interaction anisotropy [415]. In addition, Kawamura [384,416–418] has shown theoretically the possibility of a third spin-glass transition due to the decoupling of chirality with the spin for isotropic Heisenberg systems. This chiral glass (CG) phase shows several similarities with spin-glass (SG) phases, even though their origin is due to different types of frustration [384,417,418].

Based on the Raman scattering studies, Hien et al., [419] have predicted two magnetic transitions around 200 K and 80 K. In this chapter, we present evidence for a fifth glass transition in the LRO ferrimagnetic phase of BFO around 200 K using ac-susceptibility ($\chi(\omega, T)$), dc magnetization ($M(T, H)$) and neutron scattering studies on powder and single crystalline samples. The existence of this spin-glass transition around

200 K has been confirmed by history-dependent irreversibility of the zero-field cooled (ZFC) and field cooled (FC) dc M(T) curves and divergence of spin dynamics as per power-law as well as Vogel-Fulcher law using ac susceptibility measurements. Additional confirmation of the fifth spin-glass transition is presented using field (H) dependent shift of the spin-glass freezing temperature $T_f(H)$ along the Gabay-Toulouse (G-T) line, non-exponential relaxation of isothermal remanent magnetization (IRM) as a function of time and aging, rejuvenation and memory effects in the spin-glass phase. Further, it is shown that this transition is accompanied with anomalies in the intensity of *006* as well as *101* reflections. In addition, we show a drastic decrease in the intensity of the satellite peaks due to longitudinal conical order and an increase in the incommensurability of the modulation around this spin glass transition. All these observations suggest that this spin-glass transition is linked with the dynamics of spin precession in the conical magnetic structure of $BaFe_{12}O_{19}$.

7.2 Experimental

The details of the powder synthesis and single-crystal growth are given in chapter 2. The $\chi(\omega, T)$ and ZFC M(T) measurements on single crystals were carried out in the 2 to 300 K range along and perpendicular to c-axis using a SQUID-based magnetometer (MPMS-3, Quantum Design, USA). The frequency-dependent ac susceptibility ($\chi(\omega, T)$) measurements on powder samples were carried out in the temperature range 2 to 300K with an ac drive field of 3 Oe using the same set-up. Temperature-dependent M(T, H) measurements on ZFC powder samples were carried out using a physical property measurement system (PPMS) (Dynacool, Quantum Design, USA). The IRM, memory and rejuvenation effect measurements were also carried out on the powder samples of BFO using PPMS set-up. The specific heat measurements in the 1.8 K to 300 K range was also measured on the PPMS set-up.

The temperature-dependent single-crystal neutron diffraction measurements were carried out using WISH time-of-flight diffractometer at ISIS facility of the Rutherford Appleton Laboratory (RAL), United Kingdom [209].

7.3 Results and Discussion

7.3.1 Evidence for a High-Temperature Diffuse Magnetic Transition: Magnetization and Specific Heat Studies

Previous Raman scattering studies have predicted the possibility of a magnetic transition in BFO around 200K [419]. Our ZFC $M_{//c}$(T) measurements reveal the presence of a broad diffuse peak around 200 K as shown in Fig. 7.1 which depicts the results over a limited temperature range 60 to 300 K. The evidence for this transition is more clear for measurements using 1000 Oe field rather than 500 Oe field as can be seen from a comparison of the curves shown in panel (b) with panel (a). Also, the ZFC $M_{\perp c}$(T) plot, shown in panel (c), shows departure from its linear trend below 300 K around 200 K, which lies in the temperature range of the diffuse peak seen in the other two panels, particularly panel (b). This suggests the involvement of both the perpendicular and parallel components of dc magnetization in this transition. More interestingly, ZFC and FC M(T) curves bifurcate at T ≈ 250 K, as can be seen from Figs. 7.1 (b). This bifurcation temperature seems to increase with decreasing magnetic field as can be seen from a comparison of the results presented in panel (b) with those in panel (a). The bifurcation temperature reveals history-dependent irreversibility which has been reported for both spin-glass transition [57,58,60,61,245] as well as superparamagnetic (SPM) blocking transition [244]. The presence of this diffuse transition is revealed in ac $\chi'_{//c}$(T) curves also as mentioned in chapter 5 and shown again here for the 60 to 300 K range in Fig. 7.2 (a) for the sake of easy comparison. The $\chi''_{//c}$(T) curve does not reveal any marked peak below the diffuse peak temperature of ~200 K in $\chi'_{//c}$(T) but shows an

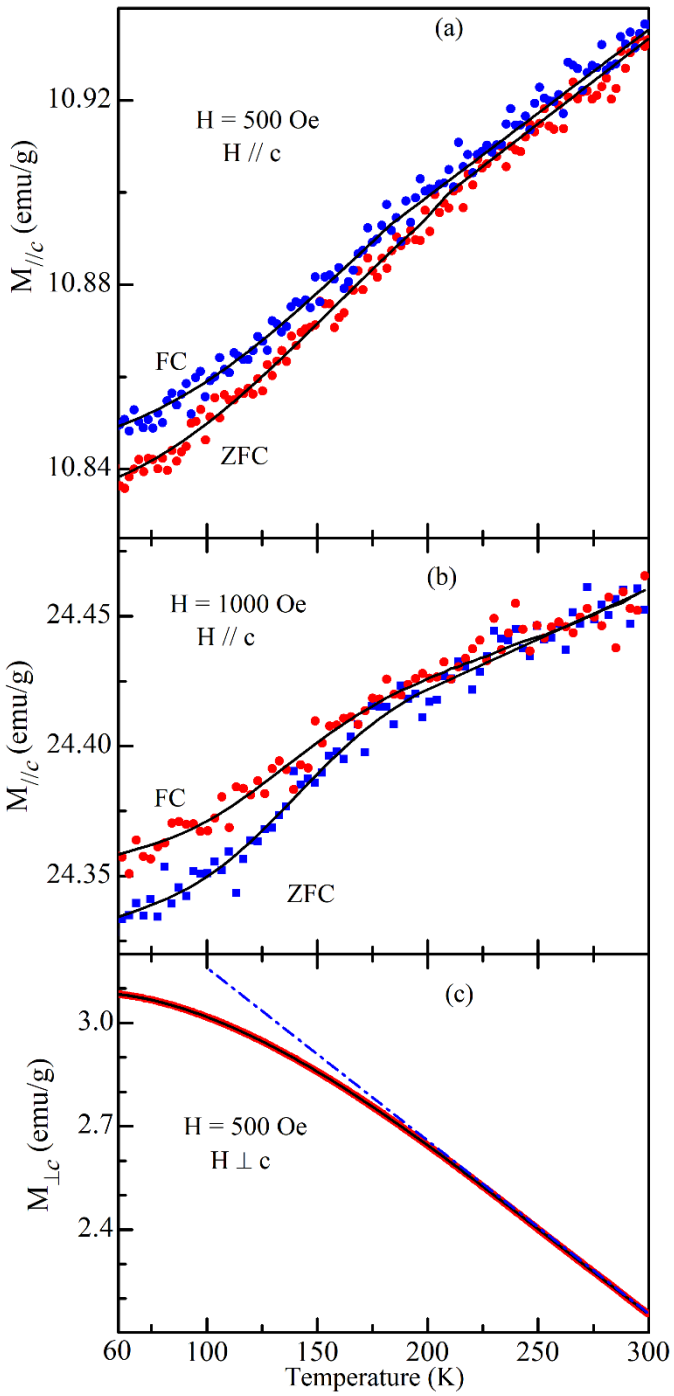

Figure 7.1: Variation of magnetization with temperature measured for a BFO single-crystal for dc fields of (a) 500 Oe and (b) 1000 Oe applied parallel to the c-axis, and (c) 500 Oe applied perpendicular to the c-axis. The continuous line through the data points are guide to the eyes, whereas the dash-dot line in (c) shows the deviation from the linear behaviour of $M_{\perp c}$ for 200 < T < 300 K. Panels (a) and (b) depict the results of both ZFC and FC measurements. Filled dots: FC and filled squares: ZFC.

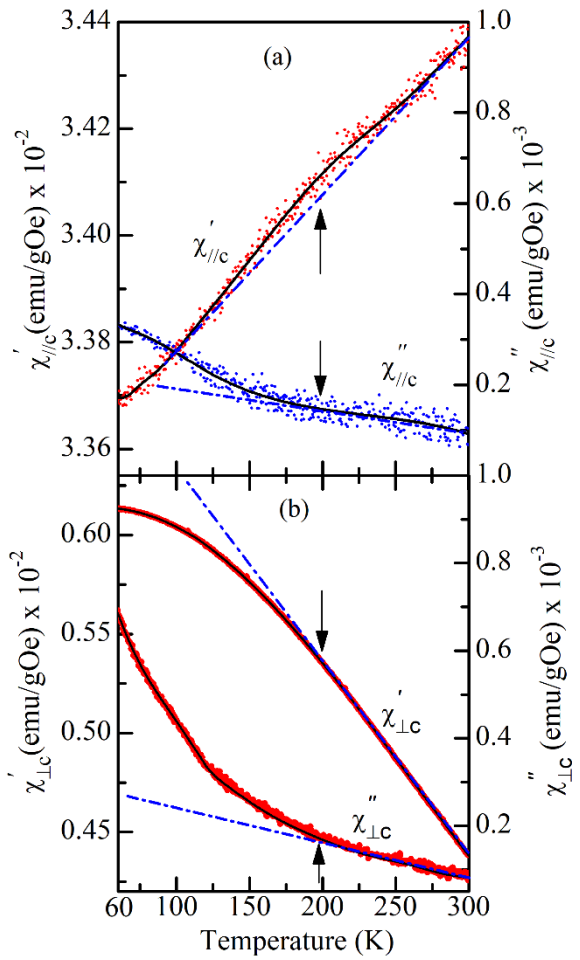

Figure 7.2: (a) Variation of $\chi'$and χ'' with temperature measured at 700 Hz and 745 Hz for an ac drive field of 3 Oe applied (a) parallel and (b) perpendicular to the c-axis, respectively. The continuous lines through the data points are guide to the eyes while the dash-dotted lines for χ''(T) curves depict departure from the linear trend below 200 K. The dashed-dotted line in $\chi'_{//c}$ in (a) has been drawn to highlight the diffuse peak superimposed over the nearly linearly decreasing trend of the background value.

abrupt rise below 200 K. Since this data is recorded at 700 Hz frequency, the peak temperature in $\chi'_{//c}(\omega, T)$ is slightly higher than that in dc ZFC $M_{//c}$(T) curves of Fig.7.1(a). As in the case of ZFC $M_{\perp c}$(T) curves, the $\chi'_{\perp c}$(T) and $\chi''_{\perp c}$(T) curves, shown in panel (b) of Fig. 7.2, also show a departure from its linear trend around the peak temperature in $\chi'_{//c}$(T). Thus, both the dc magnetization and ac susceptibility

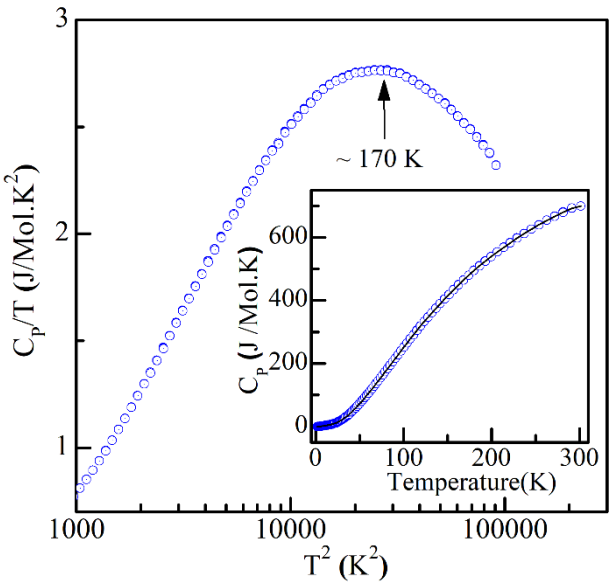

Figure 7.3: C_P/T versus T^2 semi-log plot of $BaFe_{12}O_{19}$ without any dc field bias. Inset shows the variation of C_P with temperature.

measurements reveal the occurrence of a diffuse magnetic transition with its peak in the ~ 175 to 200 K temperature range. The study of the specific heat as a function of temperature (see inset of Fig. 7.3) as such does not reveal any anomaly around 175 K. However, a plot of C_P/T versus T^2 provides robust evidence for this transition as can be seen from Fig. 7.3. More work using inelastic scattering studies (Raman, X-ray and neutron) and lattice dynamical calculations are required to understand the genesis of this transition.

7.3.2 Signature of the Diffuse Magnetic Transition in Single-Crystal Neutron Diffraction Patterns

We reproduce Fig. 5.14 of chapter 5 in the limited temperature range 60 to 300 K in Fig. 7.4. This figure depicts the variation of the integrated intensity of the *101* (panel (a)) and *006* (panel (b)) Bragg reflections in the single-crystal neutron diffraction measurements. These reflections have contribution from both nuclear as well as the magnetic structures. It is evident from this figure that the intensity of both the reflections

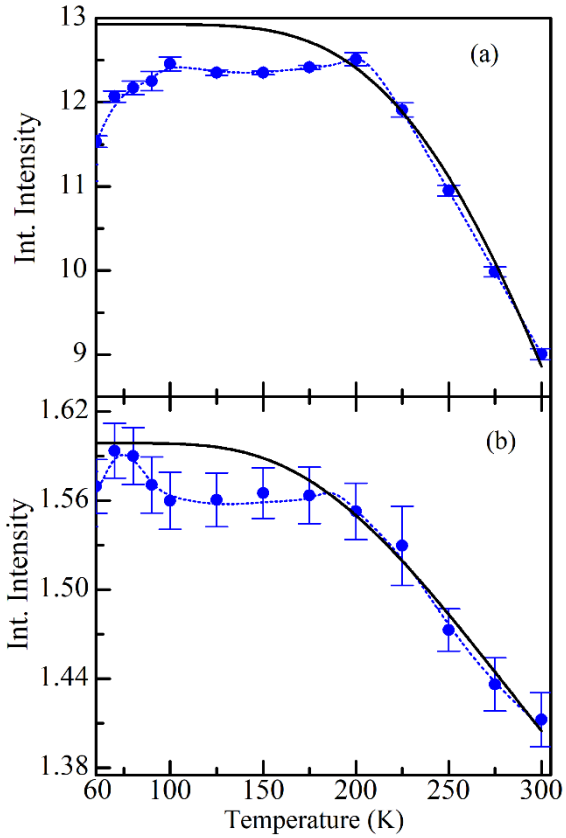

Figure 7.4: Variation of the integrated intensity of (a) *101* and (b) *006* Bragg reflections with temperature. The continuous solid line shows the Brillouin fits for the integrated intensities unlike the plotted lines through the data points are guide to the eyes.

follows the Brillouin function behaviour upto about 200 K, as shown by continuous line in the two panels. However, the observed intensity begins to decrease with respect to theoretically expected trend below this temperature suggesting detachment of some part of the spin components in both the parallel and perpendicular directions to the c-axis. As pointed out in chapter 5, such diminution of the intensity is linked with the spin-glass freezing for the other four spin-glass transitions discussed in that chapter. Since this diminution occurs in both *006* and *101* reflections, both the basal plane and c-components of the spins seem to be involved in this transition. This implies that the entire spin is involved in this transition, unlike the involvement of either in the longitudinal or the transverse components of the spins for the spin-glass transitions discussed in chapter 5

and 6. As explained below this transition is linked with the precession dynamics of the spins involved in the incommensurate longitudinal conical modulation of the underlying magnetic structure.

In chapter 3, we showed that the magnetic ground state of BFO corresponds to an incommensurate longitudinal conical modulation of the spins due to the precession of the canted spins around the c-axis, as revealed by the appearance of satellite peaks at positions forbidden by the nuclear and collinear magnetic space groups $P6_3/mmc$ and $P6_3/mm'c'$, respectively. Since the M(T), χ(T) and neutron diffraction results in Figs. 7.1, 7.2 and 7.4 reveal the involvement of the canted spin in the diffuse transition around 175 K, we explored the evolution of the magnetic satellite peaks as a function of temperature in the 1.5 K to 300 K range. Fig. 7.5 depicts the intensity profiles, recorded along the *00l* reciprocal lattice row of a BFO single-crystal around the space group forbidden 003 position, at a few selected temperatures along with the fitted profiles shown with continuous line. The two magnetic satellite peaks in this figure below and above the *003* position at (*003* - τ_1) and (*003* + τ_2) positions, respectively, are due to the longitudinal conical block modulation, while the peak centred at 003 position is most likely due to multiple scattering, even though it may also arise due to a coexisting screw-type modulation (see section 3.5.2 of chapter 3 for more details).

We focus our attention on the two satellite peaks. It is evident from Fig. 7.5 (e) that τ_1 and τ_2 are unequal at T = 1.5 K suggesting an incommensurate longitudinal modulation of the collinear magnetic structure of BFO in its ground state. With increasing temperature, τ_1 becomes nearly equal to τ_2 within the resolution of the instrument suggesting an incommensurate to commensurate transition around this temperature. The periodicity (p) of the longitudinal conical modulation at 20 K, determined from the satellite peak positions, comes out to be an integral multiple of the c-parameter of the

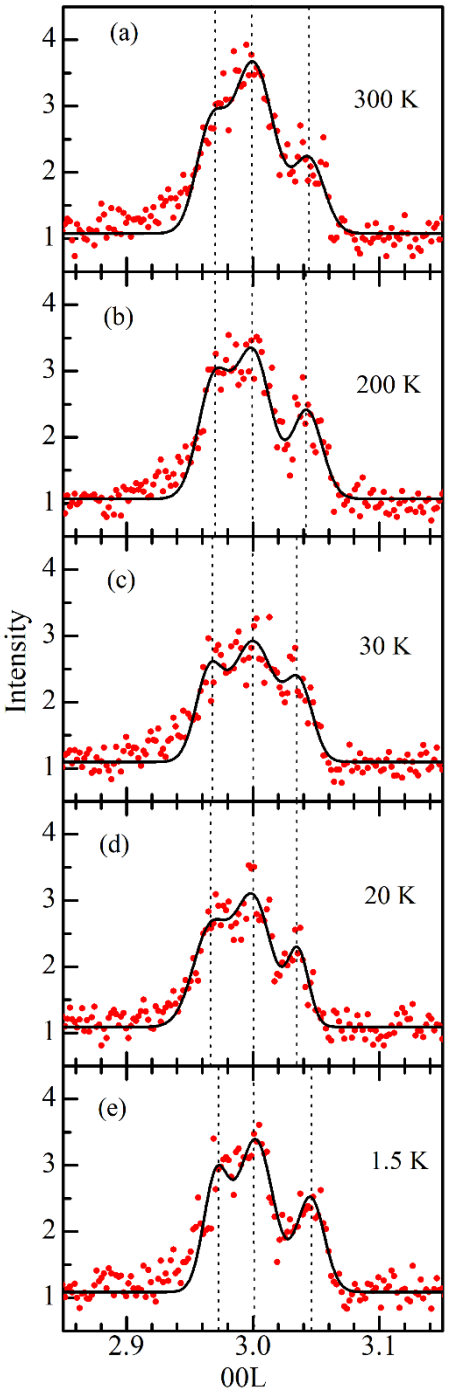

Figure 7.5: The evolution of the magnetic satellite peaks of BFO as a function of temperatures. The peak position of each satellite is marked with dotted lines. The continuous solid line through the data points is the deconvoluted profile.

underlying collinear magnetic structure. The value of p for BFO at 20 K is found to be ~ 28 c, which is much larger than the periodicity of the longitudinal conical structure reported in Sc doped BFO ($BaSc_xFe_{12-x}O_{19}$) where it varies from ~ 3.9c to 6c for Sc concentration x = 1.4 to 1.8 [132]. Thus, the conical modulation in undoped BFO is very long period one at 20 K. On increasing the temperature further, the two satellite peak positions, i.e., τ_1 and τ_2, again become unequal (see panel (b) in Fig.7.5). The variation of τ_1 and τ_2 with temperature is shown in Fig. 7.6 (a). The τ_1 and τ_2 at various temperatures

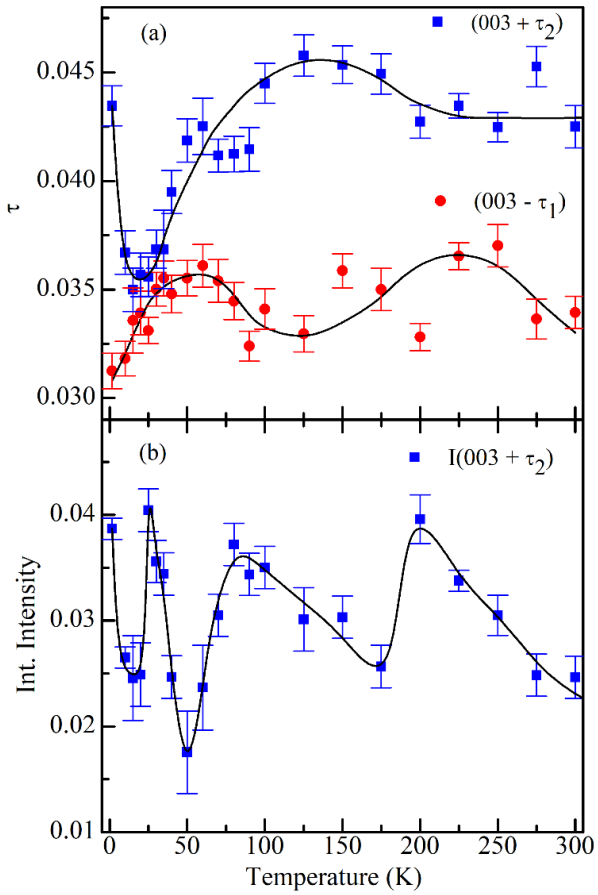

Figure 7.6: (a) The variation of the magnetic satellite peak positions, (*003* - τ_1) and (*003* + τ_2), with temperature. (b) The variation of the integrated intensity of the magnetic satellite peak at (*003* + τ_2) position with temperature. The continuous solid lines are guide to the eyes.

were obtained by deconvolution of the three peaks seen in Fig. 7.5. Coming from the higher temperature side (300 K), the τ_1 gradually increases while τ_2 is nearly temperature independent upto ~ 225 K. Such an increase in the τ_1 suggests that it tries to become equal to τ_2, as expected for an impending phase transition to a 'lock-in' phase with commensurate modulation. However, after the onset of the diffuse magnetic transition at this temperature, seen in the $M_{//c}(T)$ and $\chi'_{//c}(T)$ curves, both τ_1 and τ_2 move away from each other suggesting a reversal of the attempt to reach a commensurate τcorresponding to a 'lock-in' phase. Interestingly, at T $\lesssim$ 125 K, which coincides with the completion of the diffuse magnetic transition seen in Fig. 7.1(a)), τ_1 again begins to increase while τ_2 shows a monotonic decrease until they become nearly equal around ~ 20 K. In chapter 4, we had shown that the bandwidth of the e_g band changes abruptly around 15 K while in chapter 5 we showed that two new spin-glass transitions involving successive freezing of the longitudinal and transverse components emerging below ~ 20 K. We believe that the incommensurate to commensurate longitudinal conical transition, the reappearance of two spin-glass transitions at low temperatures (chapter 5), the change in the XMCD profile shapes (chapter 4), upturn in XMCD and $M_{\perp c}(T)$ curves (chapter 4) and the change in exchange-correlation energy (chapter 4) at T$\lesssim$ 20 K are all linked to each other. Interestingly, τ_1 and τ_2 again diverge from each other below ~ 20 K and the ground state of BFO no longer corresponds to the 'lock-in' phase but to an incommensurate modulated longitudinal conical phase at 1.2 K.

The variation of the integrated intensity of the satellite peaks, as obtained from the deconvoluted profiles, with temperature shows interesting correlation with the magnetic transition around 175 K discussed in the previous section as well as the spin-glass transitions around 50 K due to freezing of the transverse component of the spins and the two other spin-glass transitions occurring just above and below ~ 25 K discussed in

chapter 5. Fig. 7.6(b) depicts this interesting variation for the (*003* + τ_2) satellite peak. No systematic trend in the variation of the integrated intensity of the other satellite peak at (*003* - τ_1) position could be detected. It is evident from Fig. 7.6(b) that the intensity of the satellite peak at (*003* + τ_2) position first increases upto about 200 K, as expected from the increase in the magnitude of the ordered moment with decreasing temperature in the same temperature range, as revealed by the Brillouin function behaviour of the integrated intensity of the *101* and *006* Bragg peaks shown in Fig. 7.4. However, at T < 200 K, it shows a dip corresponding to the peak temperature of the diffuse transition in the $M_{//c}(T)$ plot of Fig. 7.1(b). This decrease in the intensity of the satellite peak clearly indicates that some part of the spins involved with longitudinal conical modulation is getting disordered at the diffuse magnetic transition temperature. Such a detachment of part of the spins points towards the spin-glass character of the diffuse magnetic transition, as was observed for the other four spin-glass transitions of BFO in chapter 5. Similar dips around 50 K and 25 K correlate very well with the low-temperature spin-glass transitions discussed in chapters 5 and 6.

7.3.3 Confirmation of the Spin Glass Character of the Diffuse Magnetic Transition

It is evident from the foregoing that the diffuse magnetic transition around 175 K involves both the components of spins along and perpendicular to the c-axis, even though the peak corresponding to this transition appears only in the $M_{//c}(T)$ and $\chi'_{//c}(T)$ data. In order to verify whether the irreversibility of the ZFC and FC M (T) curves shown in Fig. 7.1 is due to a spin-glass freezing or SPM blocking, we carried out a series of tests discussed in the previous chapter using measurements on polycrystalline samples. Figs. 7. 7(a) and (b) depict the dc magnetization M(T) and ac susceptibility $\chi(T)$ plots for BFO powder sample. The M(T) plot reveals a diffuse peak around 200 K (panel (a)), whereas the $\chi'(T)$ plot shows deviation from linearity around the same temperature (panel (b)). The $\chi''(T)$

plot, on the other hand, shows a diffuse peak around 160 K for a measuring frequency of 700 Hz. The temperature corresponding to the onset of increasing trend in $\chi''(T)$, shown with an arrow in panel (b) of Fig. 7.7, coincides with the temperature at which $\chi'(T)$ deviates from its linear behaviour. The temperatures T_f'' corresponding to the peak in $\chi''(T)$ as well as the onset temperature T''_{onset} show considerable frequency dispersion (see Fig. 7.8(b)) which may either be due to spin-glass freezing [57–61,245] or SPM blocking transition [244].

It is well known in the spin-glass systems that the temperature $T_f''(\omega)$ corresponding to the onset of increase in the imaginary part of ac susceptibility ($\chi''(\omega, T)$) nearly coincides with the onset of freezing revealed by the peak at $T_f'(\omega)$ in the real part

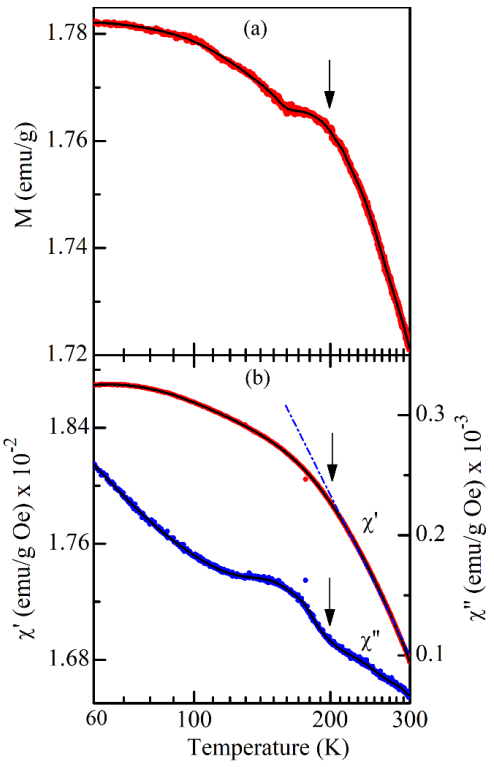

Figure 7.7: (a) Variation of magnetization measured on zero-field cooled BFO powder at 100 Oe dc field. (b) Variation of $\chi'$and χ'' with temperature measured on BFO powder at 700 Hz with an ac drive field of 3 Oe.

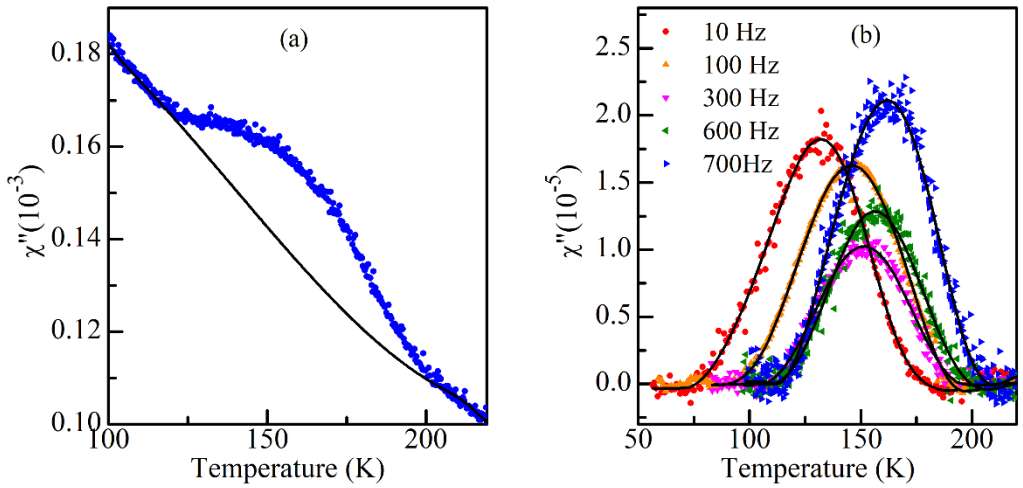

Figure 7.8: (a) The variation of χ'' with temperature at 700 Hz. The continuous line below the peak in χ'' (T) is the fitted curve for modelling the rising background value of χ'' (T) above 100 K. The panel (b) depicts the rising background-subtracted peaks in χ'' (T) at various frequencies.

of the susceptibility (i.e., $\chi'(\omega, T)$) [57,60,422,61,261–264,322,420,421]. The spin-glass freezing process at $T \leq T_f'(\omega)$ is accompanied with additional dissipation of energy and hence this rising trend followed by a peak. In the present case, the peak in $\chi''(\omega, T)$ is clearly identifiable above a monotonically rising background, as can be seen from Fig. 7.8(a) at 700 Hz. To determine the temperature corresponding to the onset of rise in $\chi''(\omega, T)$ value above the background level, we subtracted the rising background from the $\chi''(\omega, T)$ plot for each frequency. This background-subtracted peak is shown in Fig. 7.8(b) for various frequencies in the range 10 to 700 Hz. It is evident from Fig. 7.8(b) that the onset temperature T''_{onset} shifts to higher side with increasing measuring frequency. The continuous line in Fig. 7.8(b) shows the least-squares fit using a ninth order polynomial. Using the fitted curve, we determined the onset temperature $T''_{onset}(\omega)$ for further analysis.

The spin relaxation time (τ) corresponding to each $T''_{onset}(\omega)$ was determined from the usual $\omega\tau = 1$ relationship [261,264,420,423]. The variation of $\ln(\tau)$ as a function of $1/T''_{onset}$, shown in Fig. 7.9(a), is obviously non-linear ruling out the possibility of SPM

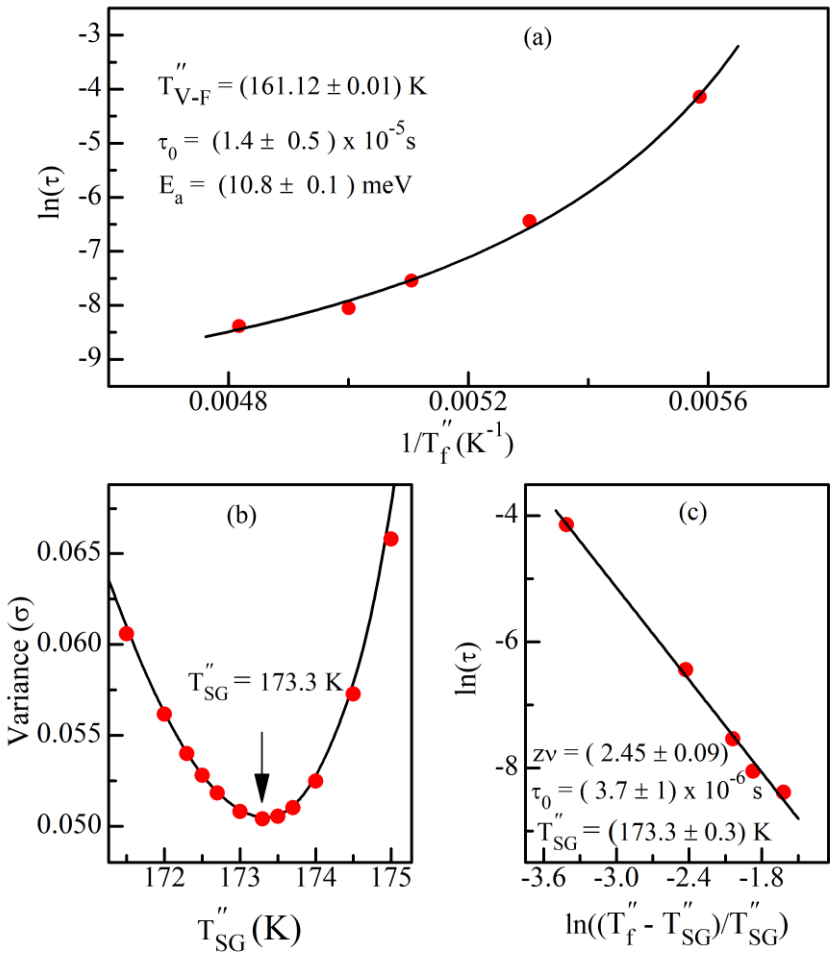

Figure 7.9: (a) Variation ln(τ) versus $1/T''_{SG}$ while the solid line is the least-squares fit for Vogel-Fulcher law. (b) Optimization of T_{SG} and (c) depicts the ln(τ) *vs* ln((T''_f − T''_{SG})/ T''_{SG}) plot along with the fit to the power-law type spin dynamics for T_{SG} = 173.3 K.

blocking for which this plot should have been linear as per Equation (5.2) (chapter 5). To confirm the spin-glass character of this transition, we modelled the temperature dependence of the relaxation time (τ) using Vogel-Fulcher law and power law discussed in chapter 5 (Equations (5.3) and (5.4)). The least-squares fit for Vogel-Fulcher law is depicted in Fig. 7.9(a) using a continuous line. This fit is quite good for the fitting parameters: T_{VF} = (161.2 ± 0.01) K, τ_0 = (1.4 ± 0.5) x10^{-5} sec and E_a = (10.8 ± 0.1) meV. For power-law behaviour, we determined the spin-glass transition temperature T_{SG} using the procedure described in chapter 5. The variation of the variance (σ) for the least-

squares fits for the power-law using various chosen values of T_{SG} shows a minimum corresponding to T_{SG} = (173.3 ± 0.03) K (see Fig. 7.9(b)). The least-squares fit for ln (τ) versus ln (($T''_{onset} - T_{SG}$)/T_{SG}) plot using T_{SG} =173.3 K is shown in Fig. 7.9(c). The value of $z\nu$ and τ_0 for this fit corresponds to (2.45 ± 0.09) and (3.7 ± 1) x10^{-6} sec, respectively. Although GoF for both Vogel-Fulcher and power laws are comparable, the spin-glass freezing temperature corresponding to divergence of τ as well as the attempt relaxation time τ_0 are somewhat different. Since it is difficult to choose one set of values over the other using GoF, we believe that the spin-glass freezing temperature T_{SG} lies somewhere in the range ~ 161 to ~ 173 K. But the most significant conclusion that can be drawn from these fits is that the diffuse magnetic transition shown in Figs. 7.1 and 7.2 is associated with breaking of the ergodic symmetry as expected for a spin-glass.

The spin-glass character of the diffuse magnetic transition was further confirmed by studying the field (H) dependence of the peak temperature in dc M(T) curves. Fig. 7.10 depicts the variation of the dc magnetization with temperature using different magnetic fields from 100 Oe to 1500 Oe. It is evident from this figure that the signature of the diffuse magnetic transition disappears for H ≥ 1000 Oe suggesting that the canted spins get aligned along the c-axis at higher fields. The transition temperatures corresponding to various fields for H < 1000 Oe was determined by using a derivative plot (dM/dT versus T) as illustrated in the inset of Fig. 7.10(d) for one measurement set. The field dependence of the diffuse magnetic transition follows G-T line with an exponent of m = 2 (see section 6.3.3 for more details about the G-T line), as can be inferred from the linear fit between T_f (H) and H^2 shown in Fig. 7.11.

As discussed in chapter 6, the spin-glass phase shows characteristic stretched exponential relaxation of thermoremanent and isothermal remanent magnetizations (TRM and IRM) as a function of time. To study this phenomenon, the powder sample of BFO

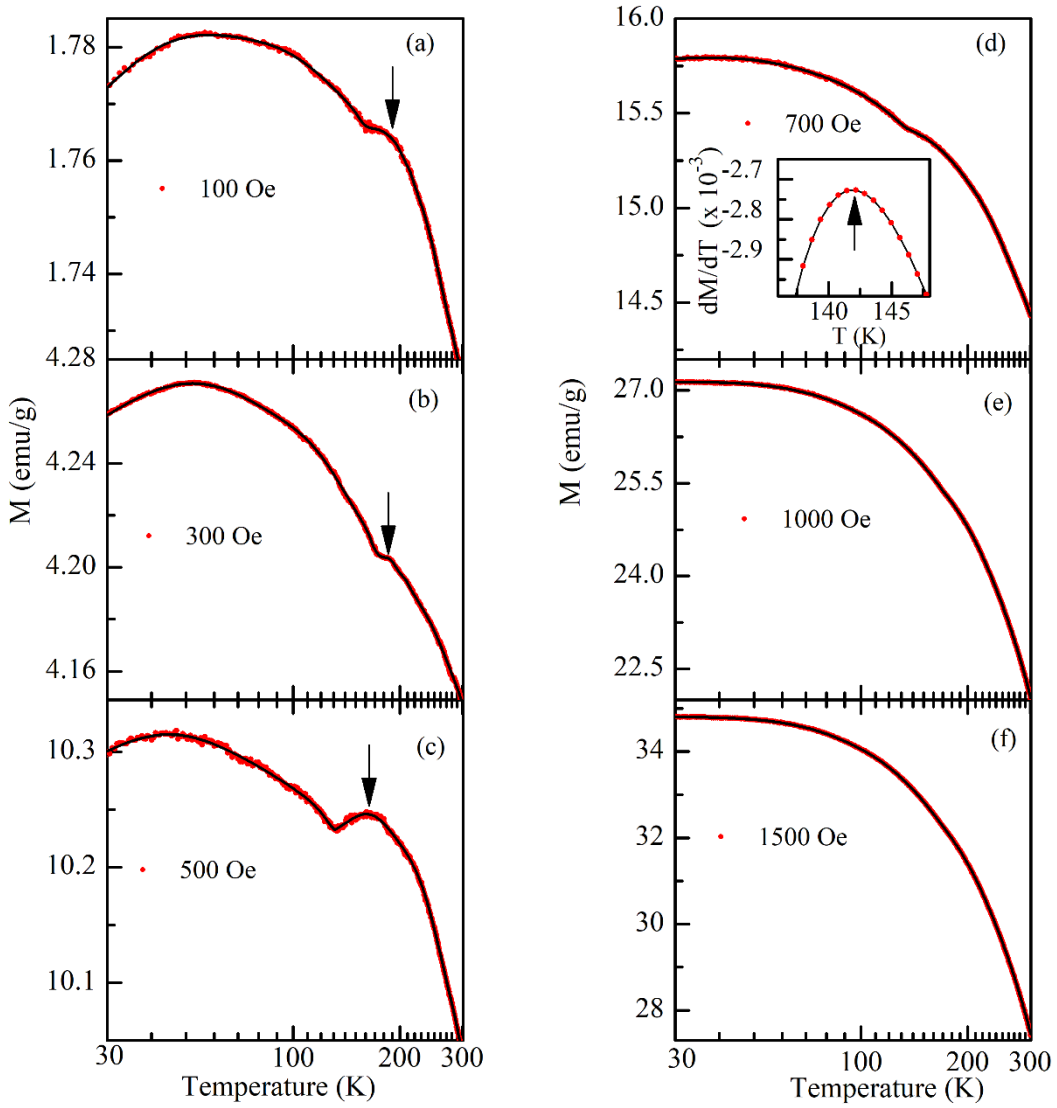

Figure 7.10: Variation of the dc magnetization of the zero-field cooled powder samples of $BaFe_{12}O_{19}$ measured during the warming cycle using a dc field of (a) 100 Oe, (b) 300 Oe, (c) 500 Oe, (d) 700 Oe, (e) 1000 Oe and (f) 1500 Oe. Arrows in (a)-(c) indicate the peak position. Inset in (d) depicts the 1st derivative of magnetization in short temperature range.

was quenched from 370 K to 100 K ($T < T_{SG}$) in zero magnetic field and then allowed to age for a wait time of $t_w = 60$ s. After the elapse of the wait time, a dc magnetic field of 50 Oe was applied and growth of the real part of ac susceptibility (i.e., $\chi'(t)$) was measured as a function of time at 200 Hz frequency using an ac drive field of 3 Oe. The results of this

measurement are shown in Fig. 7.12 where the continuous line depicts a least-squares fit for the stretched exponential function given by Equation (6.3). The fitting parameters are:

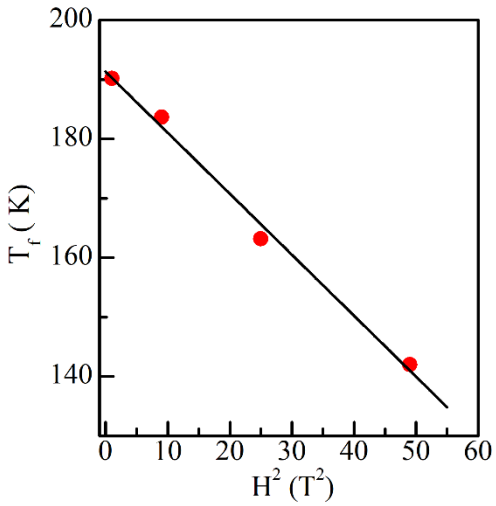

Figure 7.11: The T-H diagram showing the Gabay-Toulouse (G-T) line. The continuous line through the data points in the T-H plane is the least-squares fit to the Equation (6.2) in chapter 6.

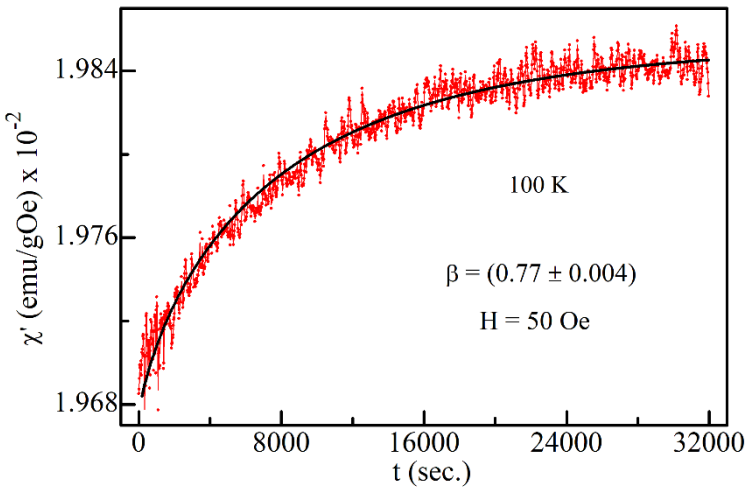

Figure 7.12: Evolution of iso-thermoremanent ac susceptibility $\chi'(\omega = 200Hz)$ with time measured at 100 K under 50 Oe dc biasing field. The solid lines through the data points is Kohlrausch-Williams-Watt (KWW) stretched exponential equation fit.

χ'_0 = (0.01985 ± 1.7 x 10^{-7}) emu/gOe, χ'_g = - (1.80 ± 0.005) x10^{-4} emu/gOe and β = (0.77 ± 0.004). The value of β so obtained suggests a non-Debye relaxation for which β should have been equal to 1. The stretched exponential behaviour of χ' (t) under IRM protocol confirms the presence of multiple minima in the energy landscape of the spin-glass state with a distribution of relaxation times, as expected for spin-glass systems [73,251,424].

We have also carried out the study of memory effects under zero-field cooled (ZFC) protocol to provide additional support for the existence of the spin-glass state. For this, the sample was initially cooled from 370 K ($T > T_{SG}$) to T_1 = 100 K ($T < T_{SG}$) under ZFC condition. After a wait time of t_w = 60 s at 100 K, evolution of the real part of ac susceptibility χ'(t) as a function of time was recorded for 8 hours at 200 Hz frequency using an ac drive field of 3 Oe in the presence of a dc bias field of H = 50 Oe [see segment "st" in Fig. 7.13]. After 8 hours, the sample was quenched to a lower temperature T_2 = 95 K, such that T_1-T_2 = 5 K, in the presence of the same dc bias field and χ'(t) evolution was again recorded over 6 hours at the same frequency and the same

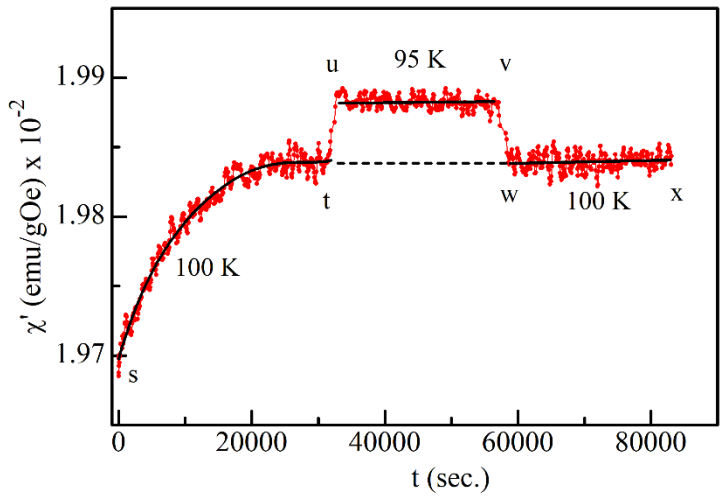

Figure 7.13: Evolution of isothermal remanent ac susceptibility χ'(ω = 200 Hz) with time measured at 100 K under 50 Oe dc biasing field measured with intermediate quenching to 95 K. The solid lines (black coloured) though the data points are guide to the eyes.

ac drive field [segment “uv” in Fig. 7.13]. Finally, the sample was heated back to T_1 = 100 K and then $\chi'(t)$ evolution was recorded for 6 hours at the same frequency, ac drive field and the dc bias field [segment “wx” in Fig. 7.13]. It is evident from Fig. 7.13 that the relaxation process during the segment “wx” is simply a continuation of the process during the segment “st”. This behaviour of $\chi'(t)$ suggests that the state of the system before cooling to T_2 = 95 K is recovered when the sample is heated back to the initial temperature i.e., T_1 = 100 K. This confirms memory effects in BFO below the highest temperature spin-glass transition of BFO.

7.4 Conclusions

The main findings of this chapter is the discovery of the fifth spin-glass transition of BFO whose signatures are seen in the M(T) and $\chi(\omega,T)$ plots of both single crystalline and powder samples. The existence of the spin-glass transition has been confirmed by the divergence of the spin relaxation time at T_{SG} and field (H) dependent shift of the spin-glass freezing temperature $T_f(H)$ along the Gabay-Toulouse line and history-dependent irreversibility of M(T). The existence of the spin-glass phase has been confirmed further by the observation of non-exponential relaxation of the isothermal remanent magnetization as well as memory effects. Single-crystal neutron diffraction studies reveal significant change in the integrated intensity of the main Bragg peaks *006* and *101* as well as the satellite peaks due to incommensurate longitudinal modulation of the magnetic structure of BFO. This spin-glass transition is most likely linked with the precession dynamics of the spins in the longitudinal conical phase of $BaFe_{12}O_{19}$ as it is accompanied with drastic decrease in the intensity of the satellite peaks.